Wang et al. *Zool. Res.* 2024, 45(3): 601−616
https://doi.org/10.24272/j.issn.2095-8137.2023.414

ZR | Zoological Research

Article Open Access

Meiotic transcriptional reprogramming mediated by cell-cell communications in humans and mice revealed by scATAC-seq and scRNA-seq

Hai-Quan Wang[1,2,#], Xiao-Long Wu[4,#], Jing Zhang[2,#], Si-Ting Wang[1], Yong-Juan Sang[5], Kang Li[2], Chao-Fan Yang[6], Fei Sun[3,*], Chao-Jun Li[1,*]

[1] *State Key Laboratory of Reproductive Medicine and Offspring Health*, *Center for Global Health*, *School of Public Health*, *Nanjing Medical University*, *Nanjing*, *Jiangsu* 211166, *China*
[2] *Medical School*, *Nanjing University*, *Nanjing*, *Jiangsu* 210093, *China*
[3] *Zhejiang University School of Medicine*, *Hangzhou*, *Zhejiang* 310016, *China*
[4] *Department of Urology and Andrology*, *Sir Run Run Shaw Hospital*, *Zhejiang University School of Medicine*, *Hangzhou*, *Zhejiang* 310000, *China*
[5] *Model Animal Research Center of Medical School*, *Nanjing University*, *Nanjing*, *Nanjing*, *Jiangsu* 210093, *China*
[6] *Liangzhu Laboratory*, *Zhejiang University*, *Hangzhou*, *Zhejiang* 311121, *China*

ABSTRACT

Meiosis is a highly complex process significantly influenced by transcriptional regulation. However, studies on the mechanisms that govern transcriptomic changes during meiosis, especially in prophase I, are limited. Here, we performed single-cell ATAC-seq of human testis tissues and observed reprogramming during the transition from zygotene to pachytene spermatocytes. This event, conserved in mice, involved the deactivation of genes associated with meiosis after reprogramming and the activation of those related to spermatogenesis before their functional onset. Furthermore, we identified 282 transcriptional regulators (TRs) that underwent activation or deactivation subsequent to this process. Evidence suggested that physical contact signals from Sertoli cells may regulate these TRs in spermatocytes, while secreted ENHO signals may alter metabolic patterns in these cells. Our results further indicated that defective transcriptional reprogramming may be associated with non-obstructive azoospermia (NOA). This study revealed the importance of both physical contact and secreted signals between Sertoli cells and germ cells in meiotic progression.

Keywords: Single-cell RNA-seq; Single-cell ATAC-seq; Spermatogenesis; Meiosis; Transcriptional reprogramming; Cell-cell communication

INTRODUCTION

Spermatogenesis is the process by which male germ cells develop into mature sperm. It involves the self-renewal and differentiation of spermatogonial stem cells (SSCs) into spermatogonia, initiation and completion of meiosis, and maturation of haploid sperm cells (Oatley & Brinster, 2012). The successful completion of spermatogenesis requires strictly orchestrated transcriptional regulation within spermatogenic cells and the coordination of the reproductive microenvironment. Despite the critical importance of spermatogenesis, our limited understanding of its underlying mechanisms impedes the management of male factor infertility, which is implicated in approximately 50% of infertility cases (Dabaja & Schlegel, 2013; Fakhro et al., 2018), with non-obstructive azoospermia (NOA) due to prophase I arrest accounting for about 35% of such cases (Soderström & Suominen, 1980).

Prophase I, constituting about 37% of total spermatogenesis, occurs strictly in chromosomal behaviors and specialized transcriptional regulation (Bolcun-Filas & Handel, 2018; Cohen et al., 2006). In mice, homologous chromosomes from parents are spatially identified and brought together to form the synaptonemal complex (SC) at leptotene (L), followed by DNA double-strand breaks (DSBs) induced by Spo11 at zygotene (Z) and pachytene (P) (Cole et al., 2010; Inagaki et al., 2010; Zickler & Kleckner, 2016). As a result of these breaks, transcriptional activity is low in the early

Received: 17 February 2024; Accepted: 27 April 2024; Online: 28 April 2024

Foundation items: This work was supported by the National Natural Science Foundation of China (82271645) and National Key Research and Development Program of China (2021YFC2700200 to F.S.)

[#]Authors contributed equally to this work

*Corresponding authors, E-mail: sunfeisrrsh@zju.edu.cn; lichaojun@njmu.edu.cn

prophase stages (leptotene, zygotene, and early pachytene), but resumes at the mid-pachytene stage (Monesi, 1964; Page et al., 2012). Subsequent research has shown that after the early pachytene stage, there is a significant down-regulation of genes associated with meiosis and an up-regulation of genes critical to spermiogenesis (Da Cruz et al., 2016). Additionally, various transcriptional regulators (TRs) have been identified as drivers of meiosis completion and fate determination of spermatocytes (Blendy et al., 1996; Don & Stelzer, 2002; Nantel et al., 1996; Wu et al., 2009). For example, *Yy1* knockout in mouse testes leads to pachytene spermatocyte arrest due to abnormal heterochromatin status and reduced global H3K9me3 levels (Wu et al., 2009). Furthermore, *Crem* knockout in mouse testes results in apoptosis of round spermatids as Crem regulates the transcription of protamine and other transition proteins specifically at pachytene, which are translated in spermatids (Blendy et al., 1996). These findings highlight crucial transcriptional reprogramming in pachytene spermatocytes in mice; however, how this reprogramming is regulated remains largely unknown.

In mammals, the physiological blood-testis barrier (BTB) helps prevent autoimmunity and provides a conducive microenvironment for spermatogenesis. Composed of three specialized cell junctions formed by adjacent Sertoli cells, including occluding junctions, anchoring junctions, and gap junctions, the BTB functionally segregates the seminiferous tubules into the basal and apical compartments (Cheng & Mruk, 2012; Gilula et al., 1976; Mruk & Cheng, 2004). In mice, syncytial spermatocytes at the pre-leptotene stage move from the basal to apical compartment, forming a temporary junction composed of Cldn3 near the basal membrane, which is subsequently replaced by Cldn11 to establish a new BTB, while the old junction is removed, releasing zygotene spermatocytes into the lumen side of the BTB (Smith & Braun, 2012). The BTB also restricts the paracellular flow of substances, including nutrients, hormones, and cellular signals (Cheng & Mruk, 2012). While the selectivity of the BTB can change the metabolic characteristics and cell fates of spermatogenic cells, its relationship with transcriptional reprogramming during meiosis has not been reported in detail.

To explore transcriptional reprogramming during meiosis, we performed single-cell ATAC-seq (scATACseq) on testicular biopsies from three healthy males aged 31, 33, and 36 years (see Materials and Methods). We also collected single-cell RNA-seq (scRNAseq) datasets of spermatogenesis from public databases (Chen et al., 2018; Guo et al., 2018; Wang et al., 2018). Our analysis revealed that this reprogramming process during prophase I was conserved across humans and mice and was modulated by notable changes in the activity of a series of TRs. These TRs may be regulated by cell-cell contact and secreted signals from Sertoli cells. Our results elucidated the transcriptional reprogramming and its underlying mechanisms in mammalian spermatogenesis.

MATERIALS AND METHODS

Ethics approval

The patients in this study provided their consent for the research (IRB Approved Protocol: TDLS-2020-36) titled “Deciphering the mechanism of chromatin and RNA alterations in male infertility”, conducted at the Male Clinic of Nantong University Medical School (Nantong, China).

Human testis sample collection and scATAC-seq library preparation

The scATAC-seq datasets were derived from samples published in our previous study (Wu et al., 2022). In brief, tissue samples from three healthy adult males (donor #1: 31 years old; donor #2: 33 years old; donor #3: 36 years old) were collected for scATAC-seq.

These individuals, alongside their wives, visited the hospital for a fertility assessment. Comprehensive examinations confirmed that these men had normal spermatogenesis and were free from abnormal karyotypes, Y chromosome micro-deletions, and any genetic anomalies linked to male infertility or sub-fertility. Furthermore, they did not suffer from chronic diseases or hypogonadotropic hypogonadism, nor had they been exposed to adjuvant hormonal therapy. The biopsies were obtained under local anesthesia, with a 0.5 cm incision made in the testicular capsule to secure a tissue sample measuring approximately 3 mm× 3 mm× 3 mm in size. This approach ensured minimal discomfort for the participants and was performed with the highest ethical standards and medical care (Wu et al., 2022).

Initially, the testicular tissue was digested into a suspension state. Cell nuclei were then extracted and prepared for sequencing based on the 10X Genomics Chromium scATAC-seq solution protocol (Cusanovich et al., 2018). For each sample, the target was to capture 15 000 nuclei. The scATAC-seq libraries were prepared according to the protocols provided by 10X Genomics and sequenced on the Illumina NovaSeq platform using PE150 sequencing. Data analysis was conducted using Cell Ranger ATAC (v.1.2.0) (Zheng et al., 2017), employing the GRCh38 genome for analysis.

Clustering, dimensionality reduction, and trajectory construction for scATAC-seq data

ArchR (v.1.0.1) (Granja et al., 2021) was employed for scATAC-seq clustering analysis, beginning with the identification of a robust set of peak regions, succeeded by iterative latent semantic indexing (LSI) dimensionality reduction. The Harmony package (v.0.1.0) (Korsunsky et al., 2019) was applied to correct for batch effects. Clustering was subsequently performed using Seurat (v.4.1.1) (Hao et al., 2021) with the FindClusters function (v.2.3) on the balanced LSI dimensions.

Cell types within each cluster were identified using gene activity scores derived from the correlation between chromatin accessibility at the gene body, promoter, and distal regulatory elements, and gene expression. ArchR calculates these gene activity scores utilizing a distance-weighted accessibility model that amalgamates the accessibility signal located within the gene body and nearby genomic regions.

To mitigate noise resulting from scATAC-seq data sparsity, we imputed the inferred gene activity scores using MAGIC85 (v.2.0.3) and conducted trajectory analysis using the *addTrajectory* function based on the gene activity score matrix.

ChromVAR deviation calculation and identification of positive TRs

The *addDeviationsMatrix* function was employed to calculate the deviations of each TR motif in every cell. These deviations provide a bias-corrected measure of how much the per-cell accessibility of a given feature (i.e., motif) deviates from its expected accessibility, based on the average across all cells or samples. Additionally, *Z*-scores, also known as deviation

scores, were calculated for further analysis.

Subsequently, ATAC-seq and RNA-seq were applied to identify TRs whose gene expression levels were positively correlated with changes in the accessibility of their corresponding motifs, designated as “positive regulators”. Specifically, ArchR was used to identify TRs where the inferred gene scores were correlated with their chromVAR (Schep et al., 2017) TR deviation *Z*-scores. Positive regulators were identified as those TRs with a correlation between motif and gene score (or gene expression) greater than 0.1, *P*-value less than 0.05, and maximum inter-cluster difference in deviation *Z*-score within the top quartile.

Sing cell RNA-seq data pre-processing

The scRNA-seq datasets used in our study were derived from the Gene Expression Omnibus (GEO) database (GSE107644, GSE120508 and GSE106487). To maintain consistency and accuracy, all datasets underwent uniform processing using the R programming language. Initially, a filter was applied to exclude any cells that contained fewer than 500 read counts to ensure data validity. Next, the count data were normalized via size factor adjustment. Logarithmic transformations on the normalized data were conducted to smooth the scale of variation and enable easier comprehension. Next, Variance Stabilizing Transformation (VST) was applied to extract the top 2 000 highly variable features (HVGs). The data were then scaled based on these 2 000 HVGs, followed by dimensionality reduction and clustering analysis using the Seurat package.

To further characterize the clusters, the *FindAllMarkers* function, which utilizes the Wilcoxon Rank Sum test, was employed. Marker genes were identified as significant based on log-fold change ($\log_2$FC)>0.5 and adjusted *P*-value<0.05 criteria.

Homologous gene conversion between species

To ensure compatibility between human and mouse data, the biomaRt package (v.2.50.3) (Durinck et al., 2009) was employed for homologous gene transformations, thereby enabling cross-species data comparability. Initially, the *useMart* function was used to access Ensembl’s Asian mirror site. Subsequently, the *getLDS* function was employed to convert mouse gene identifiers into their corresponding human homologs.

Pagoda2 analysis

To elucidate the biological state of each cell, the Pagoda2 package (v.1.0.10) (Fan et al., 2016) was used to assess gene set activity levels. The gene sets utilized in this process originated from the biological process gene sets available in the Molecular Signatures Database (MsigDB) (Subramanian et al., 2005). Initially, the expression of each gene within each cell was modeled using a mixed model that combined negative binomial and Poisson distributions, effectively handling the frequent zeros and over-dispersion encountered in scRNA-seq data. The over-dispersion of each gene was then evaluated, followed by the over-dispersion of each pathway using weighted principal component analysis (PCA). The resulting values were considered as the gene set scores for each cell.

Monocle analysis

The Monocle (v.2.22.0) R package (Trapnell et al., 2014) was used to construct single-cell trajectories. Initially, unique molecular identifier (UMI) counts were modeled using a negative binomial distribution. Subsequently, the previously identified HVGs were used as ordering genes to facilitate dimensionality reduction using the DDRTree algorithm, which preserves both the local and global structure of the data for accurate trajectory construction.

SCENIC analysis

The single-cell regulatory network inference and clustering (SCENIC) (v1.2.4) algorithm (Aibar et al., 2017) was used to elucidate the status of regulons within each cell, enabling construction of hypothetical gene regulatory networks and the definition of stable cell states. Initially, the GENIE3 algorithm was applied to predict potential regulatory networks intrinsic to each cell, focusing specifically on gene-gene interactions. Subsequently, gene regulators were identified, followed by comprehensive motif analysis using the RcisTarget package. This analysis facilitated the construction of a comprehensive network of regulons, forming a regulatory framework of TRs and their target genes. Finally, individual regulon activity within each cell was quantified using the AUCell package. This step assesses the likelihood of a particular regulon being active in a single cell, providing insight into the complex regulatory landscape of cellular states.

Cell-cell communication analysis

The R package CellChat (v.1.1.3) (Jin et al., 2021) was used to characterize cell-to-cell interactions. Following the established workflow, normalized counts were uploaded into CellChat, with standard preprocessing conducted using the *identifyOverExpressedGenes*, *identifyOverExpressedInteractions*, and *projectData* functions with specific parameters. Potential ligand-receptor interactions were then calculated using the *computeCommunProb*, *computeCommunProbPathway*, and *aggregateNet* functions with standard parameters.

Acquisition of metabolic gene sets and solute carrier transporters

Metabolic gene sets and solute carrier transporters were obtained from the Kyoto Encyclopedia of Genes and Genomes (KEGG) website (Kanehisa & Goto, 2000). Specifically, the *download.kegg* function in the ClusterProfiler package was used to download metabolic gene sets for both humans and mice. The solute carrier (SLC) molecule lists were downloaded for both humans (available at: https://www.genome.jp/kegg-bin/download_htext?htext=hsa02000&format=htext&filedir=kegg/brite/hsa) and mice (available at: https://www.genome.jp/kegg-bin/download_htext?htext=mmu02000&format=htext&filedir=kegg/brite/mmu). The AUCell algorithm was then applied to compute the activity levels of these gene sets, and the pheatmap package was used to generate heatmaps.

Functional enrichment analysis

The ClusterProfiler package (v.4.2.2) (Wu et al., 2021) was used for comprehensive functional enrichment analyses, including KEGG, Gene Ontology (GO), and Gene Set Enrichment Analysis (GSEA). This powerful tool facilitates the interpretation of biological themes among gene clusters, offering deep insights into their respective functional profiles.

RESULTS

Transcriptomic reprogramming during spermatogenesis

To elucidate the reprogramming process during

spermatogenesis in the testis, testicular tissues were collected from three healthy males and subjected to scATAC-seq using the 10X Genomics platform, as detailed in our prior publication (Wu et al., 2022) (Figure 1A; Supplementary Figure S1A). Cells with transcription start site (TSS) enrichment of less than 4 or unique fragments less than 1 000 were excluded, with the remaining cells used for subsequent analysis (Supplementary Figure S1B). Each sample yielded over 100 million total fragments (Supplementary Figure S1A, C).

Subsequently, LSI and Uniform Manifold Approximation and Projection (UMAP) were applied for dimensionality reduction of these cells, with the Leiden algorithm used to cluster them into 12 distinct groups (Figure 1B, left). Based on marker genes (Guo et al., 2018; Wang et al., 2018), the cells were further classified into five categories (Figure 1B, right). Testicular somatic cells exhibited preferential expression of *VIM*, *MYH11*, *WT1*, *ACTA2*, and *DLK1*, indicative of their role in testicular architecture and function. The SSCs were characterized by the exclusive expression of *GFRA1*, highlighting their potential for self-renewal and differentiation. Spermatogonia were identified by the expression of *MAGEA4* and *KIT*, markers that signify early germ cell development. Spermatocytes, advancing through meiosis, showed unique expression of *SPO11*, *OVOL2*, and *NME8*, reflecting their specialized role in genetic recombination and gamete formation. Lastly, spermatid cells, which are involved in the later stages of sperm development, were distinguishable by the expression of *PRM1*. The somatic cell category encompassed Sertoli, Leydig, smooth muscle, and immune cells, each contributing to the testicular environment and spermatogenesis through distinct yet complementary functions (Figure 1C).

Next, spermatocytes within the dataset were identified based on their expression profiles and subsequently classified into seven distinct subgroups. Fragment overlap on peaks in gene body regions was quantified as indicators of gene expression profiles. Based on markers of spermatocytes at each stage, these cells were classified into four groups: leptotene, zygotene, pachytene, and a mixed group of diplotene (D) and SPC7 cells (Figure 1D; Supplementary Figure S1D). Pseudotime analysis was then performed to construct a developmental trajectory. In pseudotime ordering, significant changes were observed in the accessibility patterns of genes in each stage of meiosis, especially during the transition from leptotene/zygotene (characterized by the expression of *SYCP3*, *DPH7*, *SPO11*, *SCML1*, and *SYCP2*) to pachytene/diplotene (characterized by the expression of *OVOL2* and *PRM1*) stages, suggesting a dynamic chromatin accessibility pattern from the zygotene to pachytene stages (Figure 1E).

Transcriptomic reprogramming is conserved between humans and mice

Changes in chromatin accessibility patterns are closely associated with alterations in transcriptional profiles. Therefore, previously published single-cell transcriptomic data from human testicular cells were collected for dimensionality reduction, clustering, and cell type identification (Guo et al., 2018; Wang et al., 2018) (Supplementary Figure S2A, left; Supplementary Figure S2D, left), focusing on identifying prophase I spermatocytes (Figure 2A, top). To explore similarities in the programming process between mice and humans, transcriptomic data for mouse testicular cells were also collected for analysis (Chen et al., 2018) (Figure 2A, bottom; Supplementary Figure S2A, right; Supplementary Figure S2D, right).

To assess stage-specific changes in various biological processes, gene sets related to all annotated biological processes were obtained from the GO database, with subsequent calculation of pathway scores for human and mouse spermatogenic cells using Pagoda2 and the K-means algorithm (Fan et al., 2016) (See Materials and Methods). Analysis revealed dynamic transcriptional changes during meiosis in both humans and mice (Supplementary Figure S2B, C). We subsequently identified all spermatocytes and calculated Pagoda2 scores to determine the meiotic stages where these changes occurred. Results showed that the reprogramming process occurred during the transition from zygotene to pachytene in humans, and during the pachytene stage in mice, indicating interspecies differences in the timing of this reprogramming process. Furthermore, based on the Pagoda2 scores obtained through hierarchical clustering, the biological processes were divided into two groups: one activated before reprogramming and down-regulated after reprogramming, and one exhibiting the opposite pattern (Figure 2B).

In total, 231 biological processes (20.6% of the total) were conserved in pre-reprogramming between humans and mice, including processes related to cell cycle, chromatin remodeling, and RNA stabilization, and 116 processes (19.4% of the total) were conserved in post-reprogramming, including cilium organization, acrosome assembly, and lactate metabolism (Figure 2C). As genes with low expression contributed less to the pathway scores, a human meiotic cell differentiation trajectory was constructed based on all highly variable genes and the spermatocyte cells were classified into three categories (Figure 2D): pre-reprogramming (leptotene-1, leptotene-2 and leptotene-3), reprogramming (zygotene and pachytene), and post-reprogramming cells (diplotene and SPC7). By mapping gene expression to pseudotime, three gene clusters were identified: cluster 1, activated before reprogramming and suppressed after reprogramming; cluster 2, activated during reprogramming; and cluster 3, activated after reprogramming (Figure 2E). Functional analysis of genes within these clusters revealed that cluster 1 genes were involved in RNA splicing, RNA recombination, and histone modification, cluster 2 genes were associated with cytoplasmic translation, microtubule formation, ribosome biogenesis, and RNA localization, and cluster 3 genes were related to spermatogenesis (Figure 2F). A sharp decrease in the expression levels of genes involved in synaptonemal complex formation (*SYCP1*) and chromosomal breakage and repair (*DMC1* and *MEIOB*) was observed during the reprogramming stage, whereas genes involved in flagellum formation (*DRC1* and *SPAG17*) and sperm energy metabolism (*PGK2*) exhibited a significant increase after reprogramming, despite their functionality in the round spermatid stage. Additionally, certain TRs such as *DDX25* and *RFX4*, as well as genes involved in ribosome biogenesis like *RPL29*, showed increased expression after reprogramming (Figure 2G). Immunohistochemistry results from the Human Protein Atlas (HPA) database (Uhlén et al., 2015) demonstrated high expression of DMC1 in germ cells, particularly in the pachytene stage, while DDX25 was predominantly expressed in the pachytene, diplotene, and post-meiotic germ cells (Figure 2H).

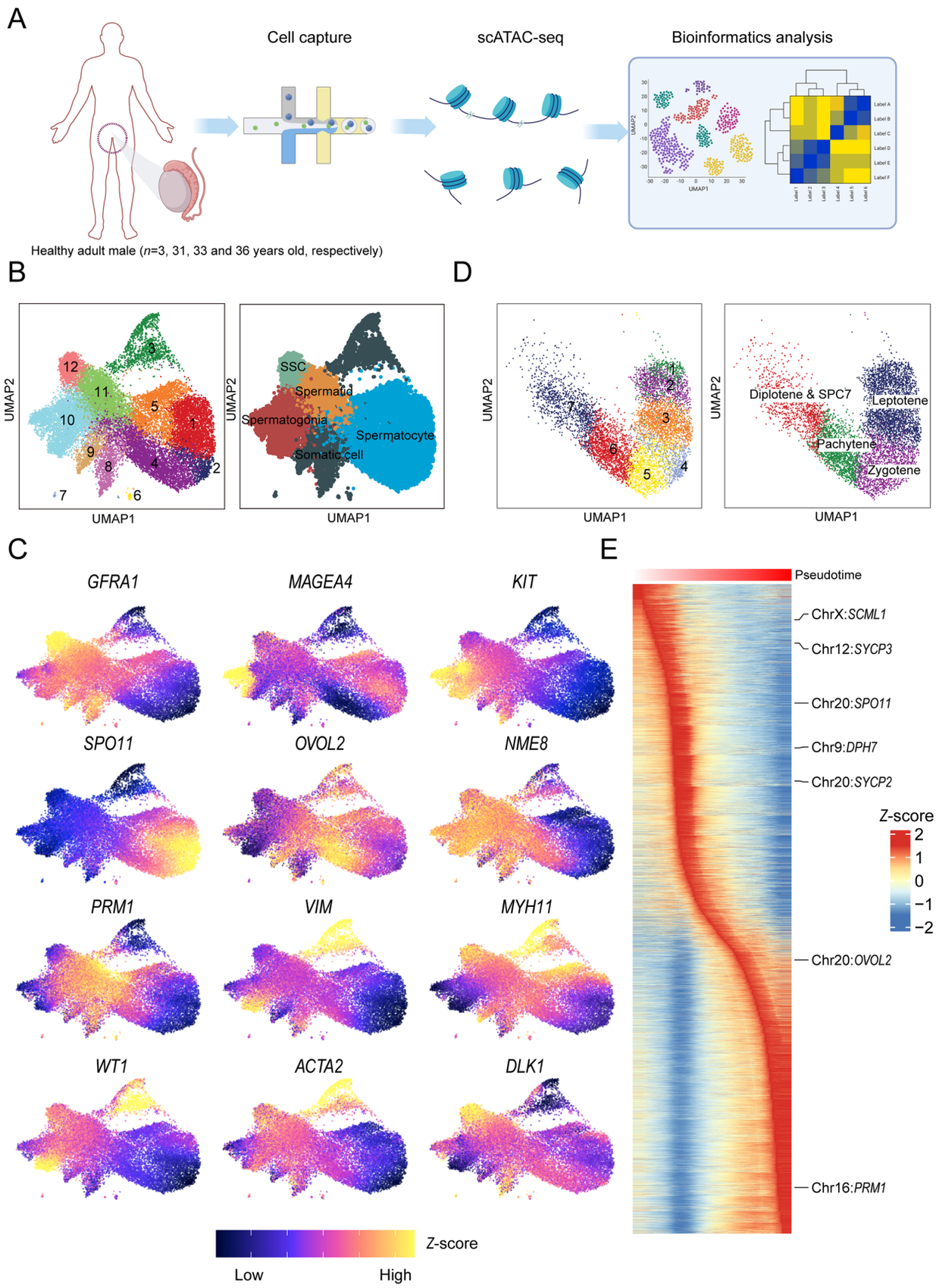

Figure 1 Transcriptomic reprogramming revealed by human testis scATAC-seq during spermatogenesis

A: Schematic of experimental workflow. B: UMAP plot showing clustering and cell population identification results. SSC, spermatogonial stem cell. C: UMAP plot showing expression of marker genes. Expression levels were transformed into *Z*-scores. D: UMAP plot showing spermatocyte clustering and identification. E: Heatmap showing accessibility of gene loci, with cells arranged in pseudotime order and accessibility values transformed into *Z*-scores.

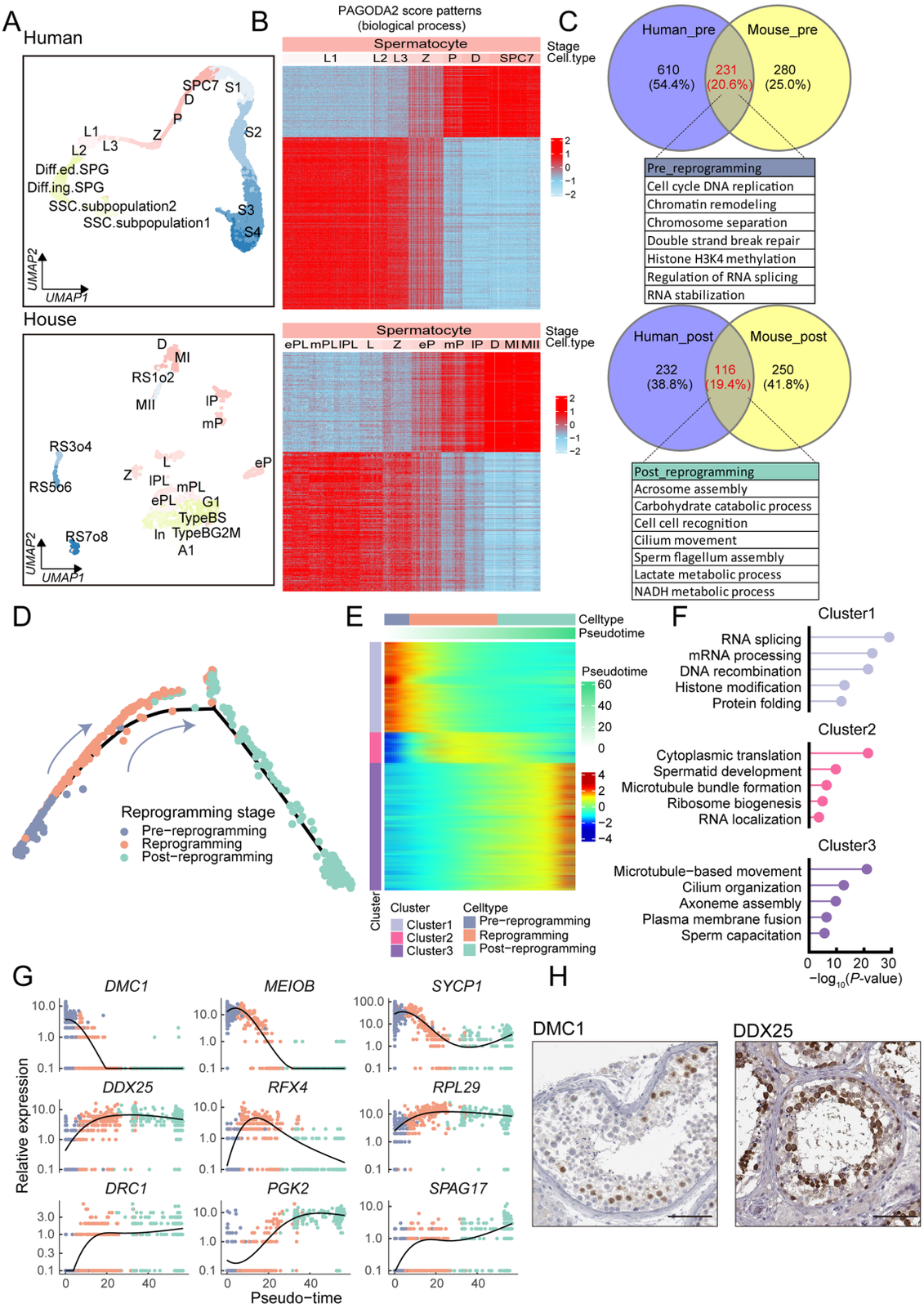

Figure 2 Transcriptomic reprogramming is conserved between humans and mice

A: UMAP showing transcriptomic profiles of human and mouse testicular cells. B: Heatmap showing Pagoda2 score patterns of biological processes from Gene Ontology (GO) database in human and mouse spermatocyte cells, with scores transformed into *Z*-scores. C: Venn diagram of conserved biological processes during reprogramming process in human and mouse spermatocyte cells. D: Trajectory plot showing differentiation of human spermatocyte cells. E: Heatmap showing gene expression levels in human spermatocyte cells, with cells arranged in pseudotime order and gene expression transformed into *Z*-scores. F: Bubble plot displaying functional analysis results of genes with different expression patterns in Figure 2E. Terms with $Q<0.05$ indicate statistically significant differences. G: Line plot showing expression changes in genes during spermatocyte differentiation during reprogramming, with each cell arranged along x-axis in pseudotime order. H: Immunohistochemical results showing expression patterns of proteins in human testicular tissue sections. Data were derived from HPA database. Scale bar: 25 μm.

In summary, our results demonstrated that transcriptional reprogramming during the transition from zygotene to pachytene occurred in both humans and mice and may be regulated by TRs.

Reprogramming process is potentially regulated by TRs

We next explored how transcriptional regulation contributes to transcriptional reprogramming in spermatocytes. The SCENIC algorithm (Aibar et al., 2017) was used to construct TR networks for both humans and mice, revealing that regulon activity changes occurred during reprogramming. This finding was consistent with our pathway analysis results (Figures 2A, 3A), suggesting that transcriptional regulation may serve as a potential mechanism underlying the reprogramming process.

Furthermore, comparative analysis of regulons between humans and mice identified 21 shared regulons between the two species, as well as 56 that were unique to humans and 103 that were unique to mice (Figure 3B). Additionally, some TRs exhibited similar activity patterns and regulated similar functions before and after reprogramming (Figure 3C). For instance, in the pre-reprogramming stage, *YY1*, *KDM5A*, *E2F1*, *E2F6*, and *BCLAF1* were activated in both humans and mice, regulating processes such as chromatin remodeling, DNA damage repair, and RNA alternative splicing. In the post-reprogramming stage, *RFX2* and *RFX4* were activated, participating in processes such as microtubule-based movement and cilium assembly. These findings suggest that stage-specific TRs may regulate the reprogramming process in spermatocytes. Additionally, the expression levels of *YY1*, *E2F1*, *RFX4*, *RFX2*, and *CREM* were validated during the reprogramming process (Figure 3E), consistent with their activation patterns. Immunohistochemical analysis using the HPA database also indicated that *E2F1* and *YY1* were mainly expressed in leptotene and zygotene spermatocytes, while *RFX2*, *RFX4*, and *CREM* were mainly expressed in pachytene spermatocytes, during meiotic division stages, and in round spermatids (Figure 3F).

To assess the potential impact of TRs on spermatogenesis, we accessed the Spermatogenesis (Zhang et al., 2013) and Meiosis online databases (https://mcg.ustc.edu.cn/bsc/meiosis/) to obtain a list of related genes, then predicted and counted the target genes from this list that could potentially be regulated by the above TRs. Results showed that *CREB1*, *KDM5B*, *CREM*, *TAF7*, and *RFX2* were the top five TRs regulating the most spermatogenic genes (Figure 3D). Previous research by Wu et al.(2016) demonstrated that spermatogenesis is blocked at the round spermatid stage in *Rfx2* knockout mice. Our results showed that *Rfx2* was active after reprogramming, suggesting that TRs activated after reprogramming may not be involved in the regulation of meiosis, but are crucial for further development of round spermatids. To confirm this, we analyzed the transcriptomic data of Wu et al.(2016) and found that the expression of a large number of *Rfx2*-target genes decreased in *Rfx2* knockout mice (Supplementary Figure S3A). Further analysis revealed that the functions of these targeted genes were related to cilium organization, including cilium assembly, cilium movement, and microtubule-based movement (Supplementary Figure S3B). Additionally, genes related to cilium organization, such as *Ccdc40*, were found to begin expression at during reprogramming (Supplementary Figure S3C). These findings indicate that certain TRs, such as *Rfx2*, play a role in the round spermatid stage rather than during meiosis.

In conclusion, our results suggested that transcriptional regulation by TRs may be a contributing factor to the occurrence of reprogramming.

Dynamic changes in accessibility in TR motifs during reprogramming

To further identify TRs involved in the reprogramming process, spermatocyte cells were isolated from the scATAC-seq data and subjected to re-clustering analysis. Similar to previous studies, the cells were categorized into pre-reprogramming, reprogramming, and post-reprogramming groups (Figure 4A). Fragment overlap on peaks in TR regions was calculated for each cell. Consistent with previous findings, specific enrichment of TRs such as *E2F6*, *E2F1*, *YY1*, *CREM*, *RFX2*, and *RFX4* was observed at different stages of reprogramming, indicating their important regulatory roles in this process (Figure 4B).

Additionally, the developmental trajectory of spermatocyte cells was constructed (Figure 4C) and motif deviation scores for these TRs were calculated (See Materials and Methods). The deviation score measures the variance from expected accessibility of a motif in a cell based on the average across all cells or samples. All measurement values of each cell were arranged in a pseudotime order, revealing a stage-specific distribution pattern of deviation scores (Figure 4D). Some TRs exhibited higher deviation scores in the pre-reprogramming stage, while others peaked during the reprogramming or post-reprogramming stages. In total, 282 TRs showed specific changes during reprogramming, with 28 TRs overlapping with previous SCENIC results, including TRs from the E2F and RFX families. These results suggested that stage-specific regulation of TRs was associated with the transcriptional reprogramming of spermatocytes (Figure 4E).

To identify the TRs potentially driving the observed changes in chromatin accessibility at their predicted binding sites, gene expression levels were estimated based on the scATAC-seq data and the correlations between gene expression and TR deviation scores were determined. TRs whose gene expression was positively correlated with changes in the accessibility of their corresponding motifs were termed “positive regulators”. Previously reported RFX family proteins, as well as previously unreported TRs such as *YBX1* and *NFYA*, were identified as positive regulators in the reprogramming process (Figure 4F). Furthermore, the expression patterns of *E2F6*, *NFYA*, and *YBX1* showed strong correlations with their deviation scores (Figure 4G).

In summary, these observations indicated significant changes in the accessibility of motifs bound by TRs during the reprogramming process, further supporting the involvement of TR regulation in the reprogramming of spermatocytes.

Physical contact signal differences in spermatogenic microenvironment during reprogramming

Spermatogenesis relies not only on intrinsic regulation within germ cells themselves but also on regulation exerted by other cells in the spermatogenic microenvironment. During spermatogenesis, Sertoli cells form the BTB through tight intercellular connections, creating an independent immune and nutritional environment for differentiating germ cells (Smith & Braun, 2012) (Figure 5A). Our results showed that, compared to zygotene spermatocytes, pachytene spermatocytes exhibited decreased expression of human leukocyte antigens (HLA-A, HLA-B, and HLA-C), as well as down-regulation of certain adhesion and junction molecules,

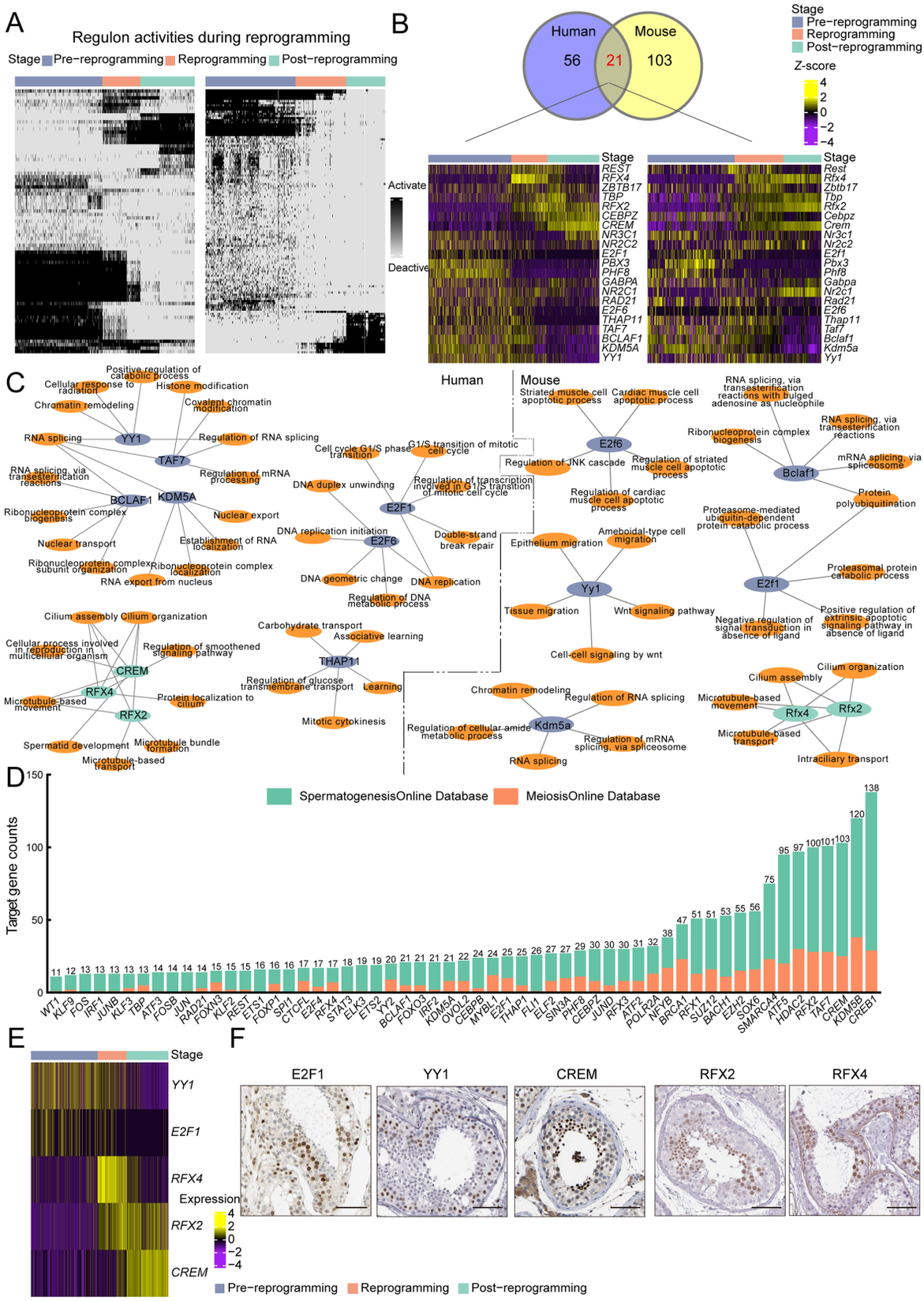

Figure 3 Reprogramming process is potentially regulated by TRs

A: Heatmap showing regulon activities of spermatocytes during reprogramming in humans and mice. B: Venn diagram showing conservation of stage-specific regulons during reprogramming between humans and mice. Heatmap showing expression of conserved TRs in spermatocytes from humans and mice. C: Network diagram showing conserved TRs during reprogramming regulated similar biological processes in humans and mice. D: Bar plot showing number of spermatogenesis-related genes regulated by conserved TRs. Genes were sourced from the Spermatogenesis and Meiosis online databases. E: Heatmap showing expression patterns of TRs in human spermatocytes. F: Immunohistochemical results showing expression patterns of TRs in human testicular tissue sections. Data were derived from HPA database. Scale bar: 25 μm.

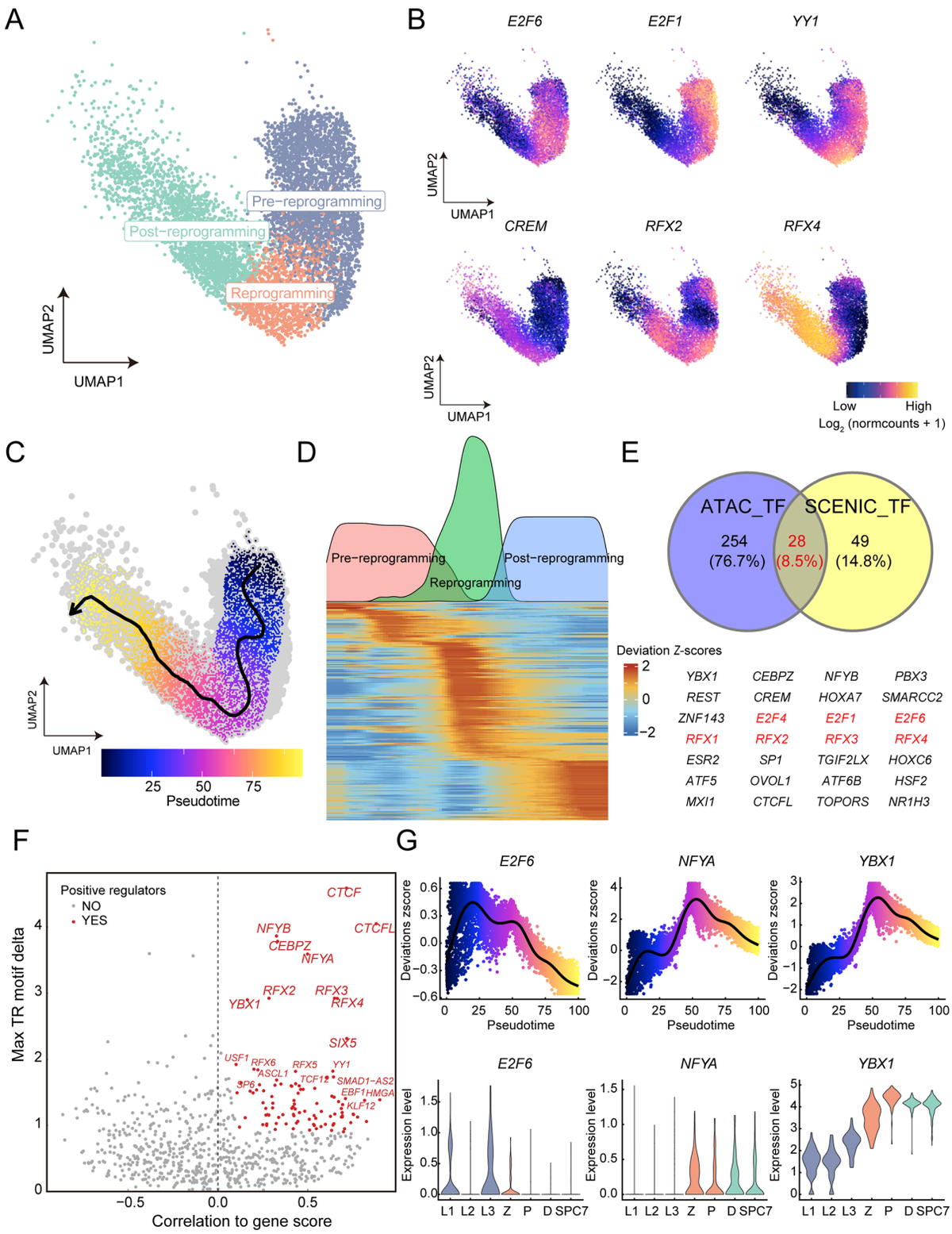

Figure 4 Dynamic changes in accessibility in TR motifs during reprogramming

A: UMAP plot illustrating clustering of human spermatocytes based on scATAC-seq data. B: UMAP plot showing accessibility of gene loci of marker genes in human spermatocytes, with colors representing log-transformed normalized count. C: UMAP plot showing differentiation trajectory of human spermatocytes. Cells not part of the trajectory are labeled “NA” and represented as gray points. D: Heatmap showing variation in deviation *Z*-scores of each TR’s motifs. Line graph above represents distribution of reprogrammed cells at each stage when cells are arranged according to pseudotime. E: Venn diagram of overlap between stage-specific TRs based on scATAC-seq data and TRs obtained using the SCENIC algorithm. Table below shows 28 overlapping TRs. F: Scatter plot showing correlation between TR expression and deviation *Z*-scores of each TR’s motifs. Positive regulators refer to those TRs whose correlation between motif and gene score (or gene expression) is greater than 0.1, with a *P*-value less than 0.05 and a maximum inter-cluster difference in deviation *Z*-score within the top quartile. G: Scatter plot showing deviation *Z*-scores of each TR’s motifs, with cells sorted according to pseudotime. Violin plot showing expression of TRs in human spermatocytes.

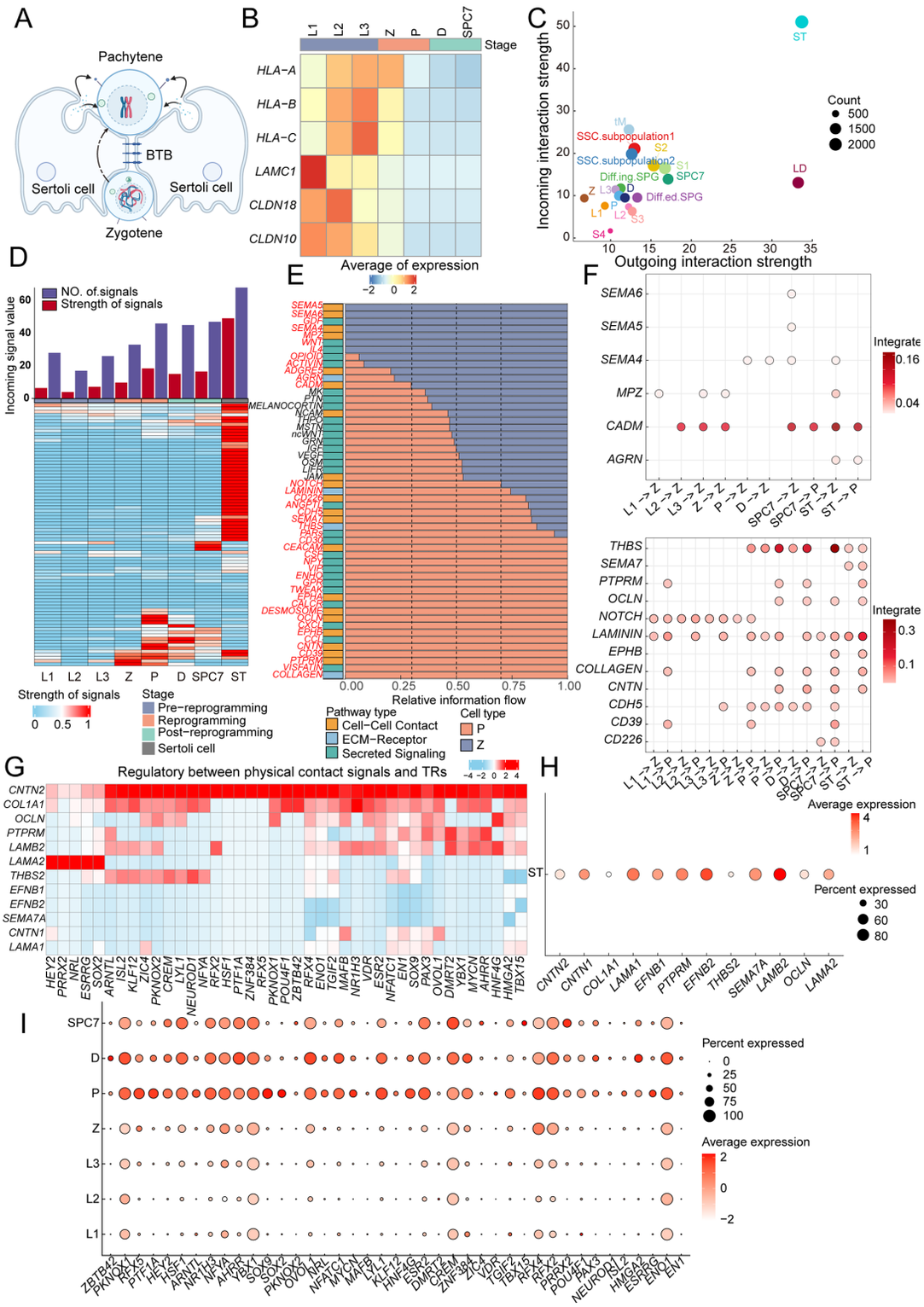

Figure 5 Physical contact signal differences in spermatogenic microenvironment during reprogramming

A: Schematic showing crossing of the blood-testis barrier (BTB) by spermatocytes in humans. B: Heatmap showing expression of human leukocyte antigen (HLA) and adhesion molecules on spermatocytes. C: Dot plot showing cell communication statistics of testicular cells, where x-axis represents total sum of outgoing signal intensity, y-axis represents total sum of incoming signal intensity, and dot size represents number of signal types. D: Heatmap showing signals received by spermatocytes at different stages, bar plot showing quantity and intensity of received signals. E: Bar plot showing relative information flow between zygotene and pachytene spermatocytes. Relative information flow of a signal greater than 0.7 represents differential information flow. F: Scatter plot showing differential information flow of physical contact signals, as depicted in Figure 5E. X-axis represents signal direction, y-axis represents signal types, and dot color represents communication possibility. G: Heatmap showing regulatory relationship between differential physical contact signals and TRs, based on the NicheNet algorithm. Color represents possibility of regulation. H: Scatterplot showing expression of differential physical contact signals in human Sertoli cells. I: Scatterplot showing expression of TRs in human spermatocytes.

such as *LAMC1*, *CLDN18*, and *CLDN10* (Figure 5B). This suggests that the immunogenicity and surface molecules of germ cells start to undergo alterations when crossing the BTB (Smith & Braun, 2012). Further analysis of the intercellular interactions between different types of germ and somatic cells using the CellChat algorithm revealed that Sertoli and Leydig cells exhibited the strongest outgoing interaction strength, while SSCs showed the strongest incoming interaction strength among germ cells. For spermatocytes, the incoming interaction strength of leptotene cells (L1 and L2) was lower than that of zygotene, pachytene, and diplotene cells, while that of L3 was comparable (Figure 5C). Subsequent ligand-receptor analysis of each cell type indicated that pachytene cells started to receive more signals than zygotene cells (Figure 5D), with a similar change in outgoing signals observed between zygotene and pachytene cells (Supplementary Figure S4A). These findings suggest that the BTB indeed affects the communication between germ cells and other cell types. To facilitate discussion, signals in the testicular microenvironment were divided into three categories: signals related to cell-cell contact, signals involved in the extracellular matrix (ECM), and secreted signals. Based on the mode of signal action, the first two categories were defined as physical contact signals.

By analyzing the information flow between zygotene and pachytene cells, we found that these two cell types received markedly different signals. Notably, physical contact signals (such as MPZ and CADM) and secreted signals (such as GDF and ACTIVIN) were received by zygotene cells more frequently than pachytene cells, whereas the opposite was true for physical contact signals (like CNTN and COLLAGEN) and secreted signals (like ENHO and NPY) (Figure 5E). Further examination indicated that signals such as SEMA4, MPZ, CADM, and AGRN exhibited stronger communication between Sertoli cells and zygotene cells than with pachytene cells. Conversely, the interactions between Sertoli cells and pachytene cells featured significantly higher signals for THBS, SEMA7, PTPRM, OCLN, LAMININ, EPHB, COLLAGEN, and CNTN compared to those observed with zygotene cells (Figure 5F). Next, the NicheNet algorithm was used to analyze the target genes of these differentially received signaling molecules in spermatocyte cells, demonstrating that previously identified TRs such as *YBX1*, *RFX4*, *RFX5*, *RFX2*, *NFYA*, and *CREM* were regulated by these signals (Figure 5G). Further analysis revealed that these signals were specifically expressed in Sertoli cells, and the predicted target genes began to exhibit high expression after reprogramming (Figure 5H, I). These results further highlighted the role of Sertoli cells in modulating transcriptional reprogramming of germ cells through intercellular interactions.

Similarly, among the signals emitted by spermatocyte cells, CADM, MPZ, EGF, and MK were found to be significantly higher in zygotene cells, while CDH5, THBS, IL4, and FGF were significantly higher in pachytene cells (Supplementary Figure S4B). Additionally, differences in outgoing signals from zygotene and pachytene cells were identified in their interactions with Sertoli cells and other spermatocytes, exhibiting significant differences between these cell types (Supplementary Figure S4C). Interestingly, the Wnt signaling pathway showed different patterns between zygotene and pachytene cells. In zygotene and earlier stages, spermatocytes primarily received Wnt signals, while in pachytene and later stages, they primarily sent Wnt signals (Supplementary Figure S4D). Further analysis demonstrated that Wnt signal receptors *FZD3* and *LRP6* exhibited higher expression in zygotene than pachytene cells, while the Wnt signal ligands *WNT2* and *WNT6* showed lower expression in zygotene than pachytene cells (Supplementary Figure S4E). These results further suggested distinct signaling communication patterns between zygotene and pachytene cells.

Secreted signals influence cellular metabolic patterns in spermatogenic microenvironment during reprogramming

In the testicular microenvironment, alongside physical cell-to-cell contact signals, secreted signals also play a pivotal role. Using the CellChat algorithm, we identified differential secreted signals in the interactions between zygotene and pachytene cells with Sertoli cells and other spermatogenic cells. Results showed that the GDF and ACTIVIN signals exchanged between zygotene and Sertoli cells were significantly stronger than those between pachytene and Sertoli cells. In contrast, the NPY and ENHO signals were stronger between pachytene and Sertoli cells than in zygotene cells (Figure 6A). Subsequent analysis showed that *NPY* and *ENHO* were primarily expressed in Sertoli cells, while their receptors, *GPR19* and *NPY5R*, began to be expressed in the pachytene phase (Figure 6B). Specifically, in the pachytene stage, spermatocytes became the primary receivers of ENHO, while SSCs and Sertoli cells were the primary senders of ENHO signals within the testis (Figure 6C). Research has shown that adropin, a peptide hormone encoded by *ENHO*, can regulate glucose homeostasis and lipid metabolism in various organs, including the liver, fat, and heart (Ali et al., 2022). Thus, we suspected that signal differences before and after the BTB may be related to metabolic shifts in spermatocytes. By evaluating the metabolic pathway scores for all spermatocytes using the AUCell algorithm, we found that while nucleotide metabolism was active during pre-reprogramming, processes such as steroid metabolism, glycolysis/gluconeogenesis, TCA cycle, and fatty acid biosynthesis increased significantly during and after reprogramming (Figure 6D). Further analysis revealed that the expression levels of facilitative GLUT transporters (*SLC2A5*, *SLC2A12*, *SLC2A13*, *SLC2A4*, and *SLC2A8*), sodium glucose cotransporters (*SLC5A2*), and fatty acid transporters (*SLC27A5* and *SLC27A6*) all increased during and after reprogramming (Figure 6E). Immunohistochemical results from the HPA database showed that the protein levels of glycolytic genes *GAPDHS* and *PGAM2*, and glucose transporters SLC2A5 and SLC2A13 were up-regulated in pachytene cells and subsequently in spermatocytes and spermatids (Figure 6F). These findings indicated that significant changes occur not only in the transcriptome but also in the metabolic patterns of either side of the BTB, highlighting the profound impact of secreted signals from Sertoli cells on the metabolic transition of spermatocytes.

Defective metabolic and transcription reprogramming in NOA patient pachytene spermatocytes

To explore potential anomalies in the spermatocyte reprogramming process in patients with NOA, two scRNA-seq datasets were downloaded from the GEO database. The first dataset originated from a patient diagnosed with pachytene spermatocyte arrest, referred to as NOA-meiosis I arrest (Huang et al., 2023), while the second dataset originated from patients diagnosed with severe oligospermia, referred to as

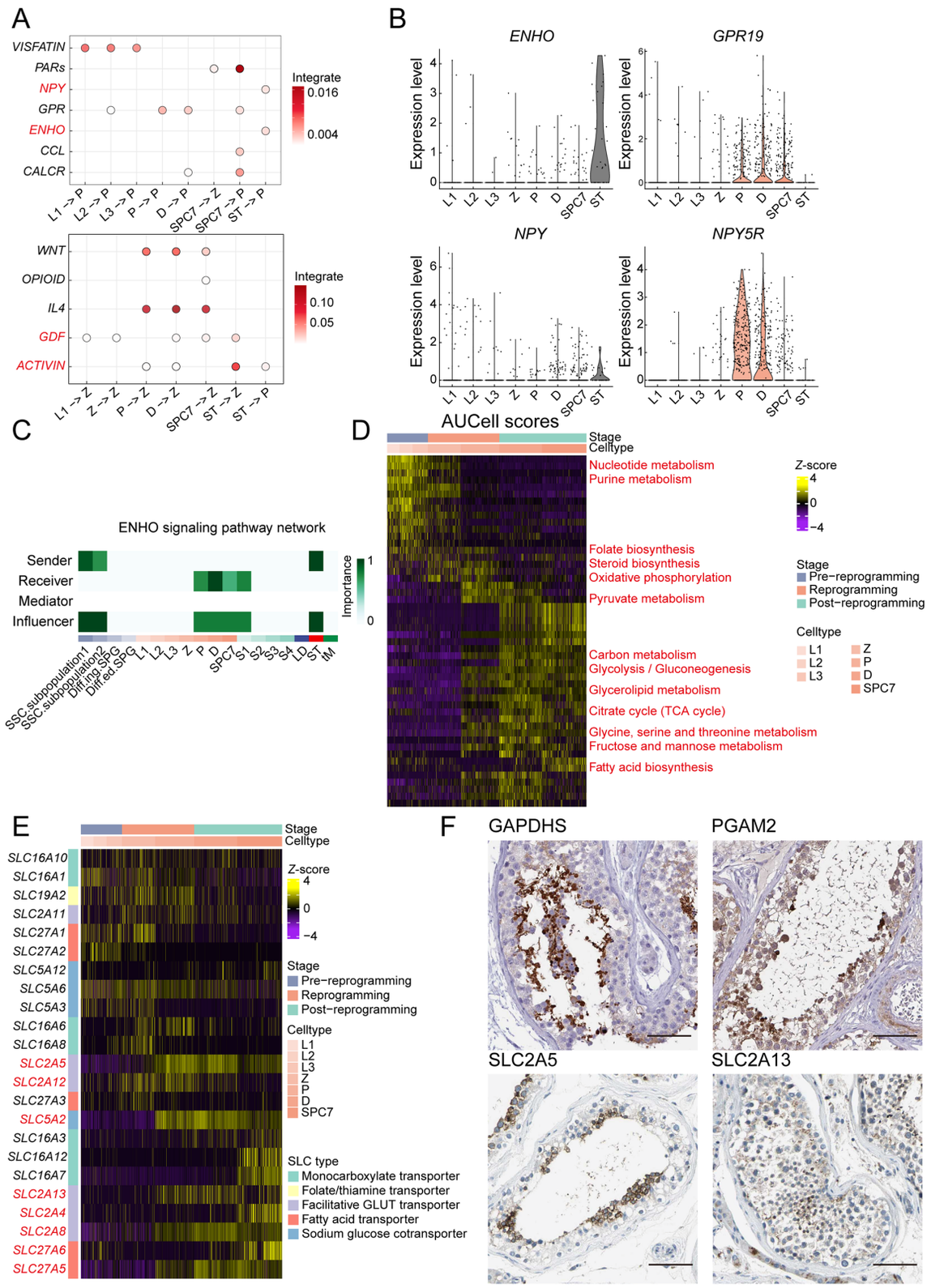

Figure 6 Secreted signals influence cellular metabolic patterns in spermatogenic microenvironment during reprogramming

A: Scatter plot showing differential information flow of secreted signals, as depicted in Figure 5E. X-axis represents signal direction, y-axis represents signal types, and dot color represents communication possibility. B: Violin plot showing expression of genes in different stages of human spermatocytes and Sertoli cells. C: Heatmap showing relative importance of each cell group based on computed four network centrality measures of ENHO signaling in human testis D: Heatmap showing metabolic pathway activity scores in human spermatocytes during reprogramming, calculated by AUCell algorithm. E: Heatmap showing expression of glucose and fatty acid transporters in human spermatocytes during reprogramming. F: Immunohistochemical results showing expression patterns of genes related to glucose metabolism and transport in human testicular tissue sections. Data were derived from HPA database. Scale bar: 25 μm.

NOA-oligospermia (Wang et al., 2021), and was collected for comparative purposes. After performing dimensionality reduction and clustering for these datasets, and using the original study's labels and known markers, 10 cell groups were identified in the NOA-meiosis I arrest dataset: two undifferentiated spermatogonia subpopulations (Undiff.SPG-1, Undiff.SPG-2), undifferentiated spermatogonia outliers consisting of Undiff.SPG-out1 (neighboring Undiff.SPG-1/2) and Undiff.SPG-out2 (close to spermatid cluster of normal samples), differentiating spermatogonia, preleptotene (preL), leptotene (L1/2/3), zygotene (Z), and prepachytene (preP) (Figure 7A, B). In the NOA-oligospermia dataset, six cell groups were identified: SSC & spermatogonia, leptotene spermatocytes, zygotene spermatocytes, pachytene spermatocytes, diplotene spermatocytes & SPC7, and spermatids (Figure 7C, D).

Next, we compared pachytene spermatocytes from healthy males and NOA patients. *GPR19* and *NPY5R*, receptors involved in the ENHO and NPY pathways (Figure 6B), showed decreased expression in all NOA datasets, especially in NOA-meiosis I arrest. ENHO plays a crucial role in maintaining the homeostasis of glucose and lipid metabolism. Accordingly, decreased expression of glucose transporters such as *SLC2A5*, *SLC2A8*, *SLC2A12*, and *SLC2A13*, and genes related to glucose metabolism was observed, indicating potential aberrations in glucose metabolism processes in the pachytene spermatocytes of NOA patients. Notably, whether in glucose transport or glucose metabolism, the expression of genes in the pachytene spermatocytes of patients with meiotic arrest was lower than that in patients with oligospermia (Figure 7E).

Additionally, we examined the expression of key TRs regulated by Sertoli cell-derived signals in pachytene spermatocytes from both healthy men and NOA patients (Figure 5I). Results suggested that these TRs were all down-regulated in NOA pachytene spermatocytes, indicating a possible disruption in signaling communication between Sertoli and germ cells (Figure 7F). This disruption likely affects the activation of crucial TRs/molecules during reprogramming, leading to abnormalities in spermatogenesis. Furthermore, pachytene spermatocytes from patients with miotic arrest generally showed lower expression of these TRs compared to those from patients with oligospermia.

In summary, these findings indicated that patients with NOA exhibit abnormalities in the expression of key genes involved in reprogramming, with more pronounced expression deficits in pachytene spermatocytes from patients with meiotic arrest than in those patients with oligospermia.

DISCUSSION

In this study, we discovered a zygotene-pachytene transcriptional alteration (ZPT) process in both humans and mice. This transcriptional reprogramming was characterized by a decrease in gene set activity related to meiosis (OC, open to close) and an increase in gene set activity related to flagellar movement and acrosome formation (CO, close to open).

Using scATAC-seq, we identified 282 TRs with changes in motif accessibility during ZPT. Among these, the motif scores for previously reported TRs, such as *CREM* and *YY1* (Blendy et al., 1996; Wu et al., 2009), varied, with the former increasing and the latter decreasing after ZPT, suggesting potential involvement in regulating this transition. Additionally, we identified previously unreported TRs that may function during ZPT, such as *YBX1*, which is involved in mRNA transcription, splicing, stability, and packaging into translationally repressed and active mRNPs (Matsumoto & Wolffe, 1998; Mordovkina et al., 2020). *YBX1* expression is reduced in testicular tissue from males with impaired spermatogenesis (Liang et al., 2021), but both the motif scores and expression of *YBX1* were increased following ZPT, suggesting a potential role in this process. Furthermore, transcriptomic analysis of testes from *Rfx2* knockout mice revealed down-regulation of target genes compared to wild-type mice, with these genes related to spermiogenesis. These results are consistent with the observed defective phenotype in the development of round sperm in *Rfx2* knockout mice (Wu et al., 2016). Additionally, based on scRNA-seq data (Chen et al., 2018; Guo et al., 2018), we found similar active patterns in TRs in humans and mice, consistent with the CO/OC pattern, with functional analysis of their target genes confirming their regulation of important spermatogenesis-related genes (Zhang et al., 2013). These results indicate that TRs are potential regulators of ZPT.

In adult humans and mice, the BTB, supported by Sertoli cells, strictly controls the flow of metabolites within the testes (Cheng & Mruk, 2012). Less differentiated cells, such as SSCs, spermatogonia, and primary spermatocytes, can directly acquire nutrients, hormones, and other biomolecules from capillaries located near the basal compartment. In contrast, highly metabolically specialized cells, such as spermatocytes and spermatids, are provided with a metabolic and immune-specific environment (Cheng & Mruk, 2012). In humans, we found that the expression of HLA molecules decreased at the pachytene stage, suggesting their transition into the apical compartment through the BTB at the pachytene stage. Additionally, we observed changes in the type and strength of cell signals among testicular cells. WNT signaling, which is associated with spermatogenesis and Sertoli cell maturation (Zhao et al., 2020), was primarily sent by germ cells after ZPT, and primarily received by germ cells before ZPT and by Sertoli cells, reflecting interactions among germ cells and between germ and Sertoli cells. Furthermore, the peptide hormone adropin has been shown to induce changes in mitochondrial fuel substrate utilization in skeletal muscle and cardiac cells, leading to increased glucose use (Thapa et al., 2018). In our study, *ENHO*, the gene encoding adropin, was highly expressed in Sertoli cells, and its receptor *GPR19* was expressed post-ZPT, coinciding with increased glucose utilization after ZPT. These findings indicate that Sertoli cells play an important role in regulating the metabolic patterns of germ cells and potentially influence TRs through their signaling.

In patients with NOA, prophase I arrest accounts for approximately 35% of all cases (Soderström & Suominen, 1980). In this study, we explored whether spermatocyte reprogramming in NOA patients exhibits abnormalities. Our results revealed distinct cellular compositions in the testes of patients with pachytene spermatocyte arrest (NOA-meiosis I arrest) and severe oligospermia (NOA-oligospermia), indicating potential disparities in spermatogenic progression between these conditions. Notably, the expression levels of GPR19 and NPY5R, receptors involved in the ENHO and NPY pathways, were markedly decreased across all NOA datasets, particularly in NOA-meiosis I arrest patients. As ENHO is essential for maintaining metabolic homeostasis, its impaired

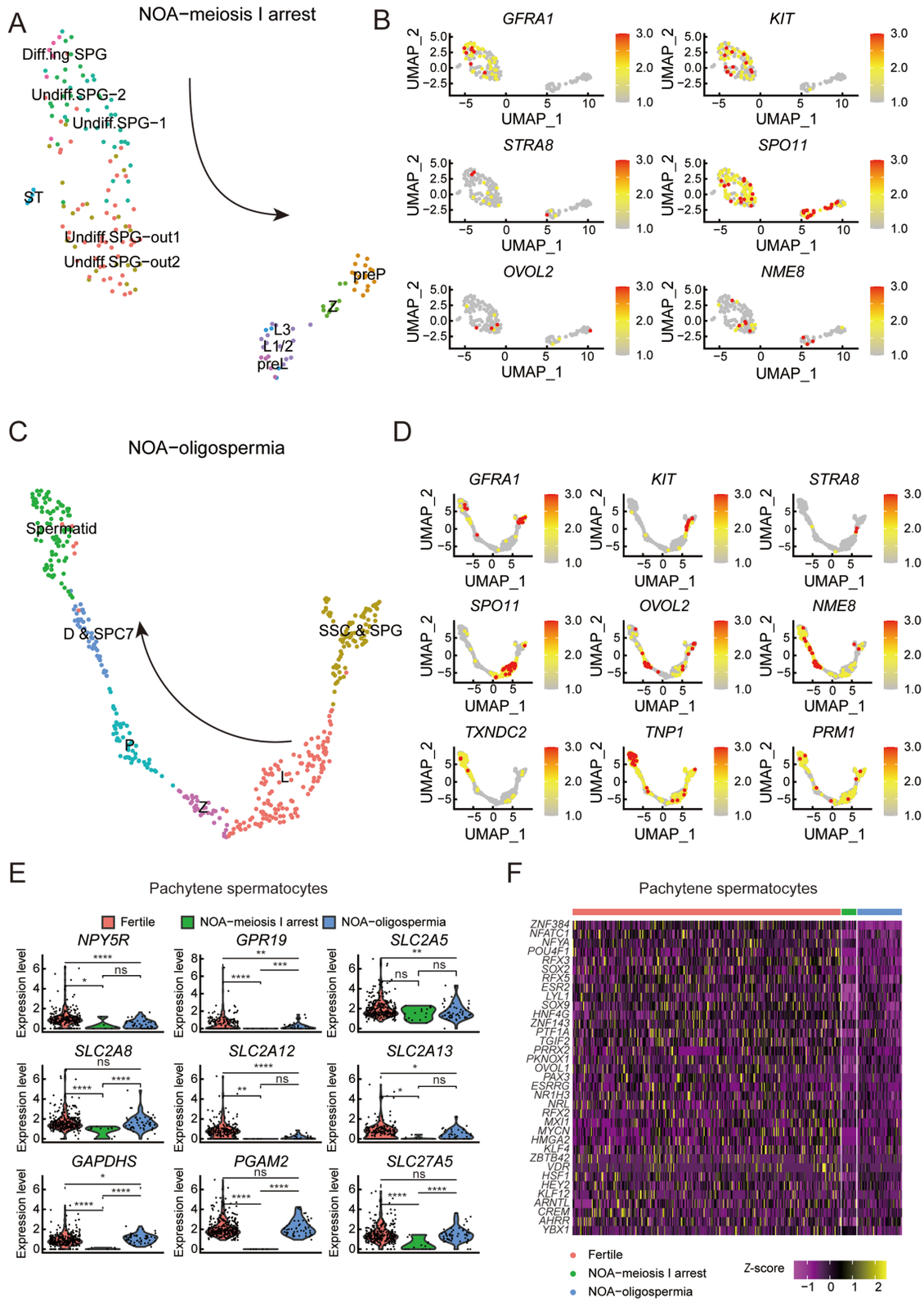

Figure 7 Defective metabolic and transcription reprogramming in NOA patient pachytene spermatocytes

A: UMAP plot showing spermatogenic cells from a patient with meiotic I arrest (GSE235321, NOA1, pachytene spermatocyte arrest). B: UMAP plots showing expression levels of marker genes across different cell types identified in the spermatogenesis process in the testis of the patient with meiotic arrest. C: UMAP plot showing spermatogenic cells from an oligospermia patient (GSE157421). D: UMAP plot showing expression levels of marker genes across different cell types identified in the spermatogenesis process in the testis of the oligospermia patient. E: Violin plot of genes from Figure 6B and 6E, comparing expression levels among the three groups (fertile, meiosis I arrest and oligospermia) within pachytene spermatocytes. Results were analyzed using *t*-test, where $P<0.05$ was considered statistically significant. ns: Not significant; *: $P<0.05$; **: $P<0.01$; ***: $P<0.001$; ****: $P<0.0001$. F: Heatmap showing expression levels of numerous TRs from Figure 5I in pachytene spermatocytes of fertile, meiosis I arrest, and oligospermia patients. Color scale on the right represents *Z*-score values.

signaling suggests a fundamental metabolic disruption in spermatocyte reprogramming within NOA, as supported by the observed down-regulation of several glucose transporters and glucose metabolism-related genes in the pachytene spermatocytes of NOA patients, especially in those with meiotic arrest. These metabolic aberrations may underpin the spermatogenic defects observed in NOA, potentially through energy deficits that impact spermatocyte viability and function. Our findings also indicated a possible breakdown in communication between Sertoli and germ cells in NOA patients, as evidenced by the down-regulation of key TRs. This disruption may impede the proper activation of TRs necessary for successful reprogramming of spermatocytes during spermatogenesis, leading to the observed defects in cell differentiation and maturation. Overall, our results revealed significant impairments in both metabolic and transcriptional reprogramming in the testes of NOA patients, particularly those with meiotic arrest, likely contributing to spermatogenic failures and suggesting that targeted interventions aimed at restoring metabolic and transcriptional balance could be beneficial for treating this form of male infertility.

In somatic and oocyte cells, mitosis and meiosis DNA damage checkpoints ensure that any damaged or incompletely replicated DNA is sufficiently repaired before division, preventing apoptosis and death from unrepaired DNA (Pan & Li, 2019; Sen & Caiazza, 2013). However, similar mechanisms have not been extensively documented in male spermatogenesis. Our findings suggest that between the zygotene and pachytene stages, where DSBs occur and DNA repair ensues, significant transcriptional changes are critical. If these changes are disrupted, spermatogenesis may become abnormal and arrest. Thus, it can be hypothesized that the zygotene to pachytene transition serves as a vital checkpoint in spermatogenesis, reliant on the successful completion of ZPT.

In conclusion, we identified a crucial transcriptional reprogramming during spermatogenesis in mammals, occurring from the zygotene to pachytene stage, driven by the reproductive microenvironment and regulated by TRs.

DATA AVAILABILITY

All scRNA-seq data mentioned in this article were obtained from the GEO public database (see corresponding citations in this article for GEO IDs). The human testicular scATAC-seq data were from our previous work (Wu et al., 2022), available in the SRA database (https://www.ncbi.nlm.nih.gov/sra/PRJNA889390).

SUPPLEMENTARY DATA

Supplementary data to this article can be found online.

COMPETING INTERESTS

The authors declare that they have no competing interests.

AUTHORS' CONTRIBUTIONS

C.J.L. and F.S. designed and supervised the experiments; F.S. and X.L.W. prepared the clinical samples; H.Q.W., X.L.W., K.L., Y.J.S., S.T.W., and C.F.Y downloaded and analyzed the human and mouse testicular scRNA-seq data; H.Q.W., J.Z., and X.L.W. performed scATAC-seq analysis; H.Q.W., X.L.W., and J.Z. wrote the manuscript. All authors read and approved the final version of the manuscript.

ACKNOWLEDGMENTS

We thank Dr. Jian-Ming Zeng (University of Macau), Dr. Jun Zhang (China Pharmaceutical University), and all members of the bioinformatics team Biotrainee for generously sharing their experience and codes.

REFERENCES

Aibar S, González-Blas CB, Moerman T, et al. 2017. SCENIC: single-cell regulatory network inference and clustering. Nature Methods, 14(11): 1083–1086.

Ali II, D'souza C, Singh J, et al. 2022. Adropin's role in energy homeostasis and metabolic disorders. International Journal of Molecular Sciences, 23(15): 8318.

Blendy JA, Kaestner KH, Weinbauer GF, et al. 1996. Severe impairment of permatogenesis in mice lacking the CREM gene. Nature, 380(6570): 162–165.

Bolcun-Filas E, Handel MA. 2018. Meiosis: the chromosomal foundation of reproduction. Biology of Reproduction, 99(1): 112–126.

Chen Y, Zheng YX, Gao Y, et al. 2018. Single-cell RNA-seq uncovers dynamic processes and critical regulators in mouse spermatogenesis. Cell Research, 28(9): 879–896.

Cheng CY, Mruk DD. 2012. The blood-testis barrier and its implications for male contraception. Pharmacological Reviews, 64(1): 16–64.

Cohen PE, Pollack SE, Pollard JW. 2006. Genetic analysis of chromosome pairing, recombination, and cell cycle control during first meiotic prophase in mammals. Endocrine Reviews, 27(4): 398–426.

Cole F, Keeney S, Jasin M. 2010. Evolutionary conservation of meiotic DSB proteins: more than just Spo11. Genes & Development, 24(12): 1201–1207.

Cusanovich DA, Hill AJ, Aghamirzaie D, et al. 2018. A single-cell atlas of *in vivo* mammalian chromatin accessibility. *Cell*, **174**(5): 1309–1324. e18.

da Cruz I, Rodríguez-Casuriaga R, Santiñaque FF, et al. 2016. Transcriptome analysis of highly purified mouse spermatogenic cell populations: gene expression signatures switch from meiotic-to postmeiotic-related processes at pachytene stage. BMC Genomics, 17: 294.

Dabaja AA, Schlegel PN. 2013. Microdissection testicular sperm extraction: an update. Asian Journal of Andrology, 15(1): 35–39.

Don J, Stelzer G. 2002. The expanding family of CREB/CREM transcription factors that are involved with spermatogenesis. Molecular and Cellular Endocrinology, 187(1-2): 115–124.

Durinck S, Spellman PT, Birney E, et al. 2009. Mapping identifiers for the integration of genomic datasets with the R/Bioconductor package biomaRt. Nature Protocols, 4(8): 1184–1191.

Fakhro KA, Elbardisi H, Arafa M, et al. 2018. Point-of-care whole-exome sequencing of idiopathic male infertility. Genetics in Medicine, 20(11): 1365–1373.

Fan J, Salathia N, Liu R, et al. 2016. Characterizing transcriptional heterogeneity through pathway and gene set overdispersion analysis. Nature Methods, 13(3): 241–244.

Gilula NB, Fawcett DW, Aoki A. 1976. The Sertoli cell occluding junctions and gap junctions in mature and developing mammalian testis. Developmental Biology, 50(1): 142–168.

Granja JM, Corces MR, Pierce SE, et al. 2021. ArchR is a scalable software package for integrative single-cell chromatin accessibility analysis. Nature Genetics, 53(3): 403–411.

Guo JT, Grow EJ, Mlcochova H, et al. 2018. The adult human testis transcriptional cell atlas. Cell Research, 28(12): 1141–1157.

Hao YH, Hao S, Andersen-Nissen E, et al. 2021. Integrated analysis of multimodal single-cell data. *Cell*, **184**(13): 3573–3587. e29.

Huang YP, Li L, An G, et al. 2023. Single-cell multi-omics sequencing of human spermatogenesis reveals a DNA demethylation event associated with male meiotic recombination. Nature Cell Biology, 25(10): 1520–1534.

Inagaki A, Schoenmakers S, Baarends WM. 2010. DNA double strand break repair, chromosome synapsis and transcriptional silencing in meiosis. Epigenetics, 5(4): 255–266.

Jin SQ, Guerrero-Juarez CF, Zhang LH, et al. 2021. Inference and analysis of cell-cell communication using CellChat. Nature Communications, 12(1): 1088.
Kanehisa M, Goto S. 2000. KEGG: kyoto encyclopedia of genes and genomes. Nucleic Acids Research, 28(1): 27–30.
Korsunsky I, Millard N, Fan J, et al. 2019. Fast, sensitive and accurate integration of single-cell data with Harmony. Nature Methods, 16(12): 1289–1296.
Liang JY, Zheng YC, Zeng WH, et al. 2021. Comparison of proteomic profiles from the testicular tissue of males with impaired and normal spermatogenesis. Systems Biology in Reproductive Medicine, 67(2): 127–136.
Matsumoto K, Wolffe AP. 1998. Gene regulation by Y-box proteins: coupling control of transcription and translation. Trends in Cell Biology, 8(8): 318–323.
Monesi V. 1964. Ribonucleic acid synthesis during mitosis and meiosis in the mouse testis. Journal of Cell Biology, 22(3): 521–532.
Mordovkina D, Lyabin DN, Smolin EA, et al. 2020. Y-box binding proteins in mRNP assembly, translation, and stability control. Biomolecules, 10(4): 591.
Mruk DD, Cheng CY. 2004. Sertoli-sertoli and sertoli-germ cell interactions and their significance in germ cell movement in the seminiferous epithelium during spermatogenesis. Endocrine Reviews, 25(5): 747–806.
Nantel F, Monaco L, Foulkes NS, et al. 1996. Spermiogenesis deficiency and germ-cell apoptosis in CREM-mutant mice. Nature, 380(6570): 159–162.
Oatley JM, Brinster RL. 2012. The germline stem cell niche unit in mammalian testes. Physiological Reviews, 92(2): 577–595.
Page J, de la Fuente R, Manterola M, et al. 2012. Inactivation or non-reactivation: what accounts better for the silence of sex chromosomes during mammalian male meiosis. Chromosoma, 121(3): 307–326.
Pan B, Li JL. 2019. The art of oocyte meiotic arrest regulation. Reproductive Biology and Endocrinology, 17(1): 8.
Schep AN, Wu BJ, Buenrostro JD, et al. 2017. chromVAR: inferring transcription-factor-associated accessibility from single-cell epigenomic data. Nature Methods, 14(10): 975–978.
Sen A, Caiazza F. 2013. Oocyte maturation: a story of arrest and release. Frontiers in Bioscience, 5(2): 451–477.
Smith BE, Braun RE. 2012. Germ cell migration across sertoli cell tight junctions. Science, 338(6108): 798–802.
Soderström KO, Suominen J. 1980. Histopathology and ultrastructure of meiotic arrest in human spermatogenesis. Archives of Pathology & Laboratory Medicine, 104(9): 476–482.
Subramanian A, Tamayo P, Mootha VK, et al. 2005. Gene set enrichment analysis: a knowledge-based approach for interpreting genome-wide expression profiles. Proceedings of the National Academy of Sciences of the United States of America, 102(43): 15545–15550.
Thapa D, Stoner MW, Zhang ML, et al. 2018. Adropin regulates pyruvate dehydrogenase in cardiac cells via a novel GPCR-MAPK-PDK4 signaling pathway. Redox Biology, 18: 25–32.
Trapnell C, Cacchiarelli D, Grimsby J, et al. 2014. The dynamics and regulators of cell fate decisions are revealed by pseudotemporal ordering of single cells. Nature Biotechnology, 32(4): 381–386.
Uhlén M, Fagerberg L, Hallström BM, et al. 2015. Tissue-based map of the human proteome. Science, 347(6220): 1260419.
Wang M, Liu XX, Chang G, et al. 2018. Single-cell RNA sequencing analysis reveals sequential cell fate transition during human spermatogenesis. *Cell Stem Cell*, **23**(4): 599–614. e4.
Wang M, Xu YW, Zhang YC, et al. 2021. Deciphering the autophagy regulatory network via single-cell transcriptome analysis reveals a requirement for autophagy homeostasis in spermatogenesis. Theranostics, 11(10): 5010–5027.
Wu S, Hu YC, Liu HF, et al. 2009. Loss of YY1 impacts the heterochromatic state and meiotic double-strand breaks during mouse spermatogenesis. Molecular and Cellular Biology, 29(23): 6245–6256.
Wu TZ, Hu EQ, Xu SB, et al. 2021. clusterProfiler 4.0: a universal enrichment tool for interpreting omics data. The Innovation, 2(3): 100141.
Wu XL, Lu MJ, Yun DM, et al. 2022. Single-cell ATAC-Seq reveals cell type-specific transcriptional regulation and unique chromatin accessibility in human spermatogenesis. Human Molecular Genetics, 31(3): 321–333.
Wu YJ, Hu XJ, Li Z, et al. 2016. Transcription factor RFX2 is a key regulator of mouse spermiogenesis. Scientific Reports, 6: 20435.
Zhang YW, Zhong LW, Xu B, et al. 2013. SpermatogenesisOnline 1.0: a resource for spermatogenesis based on manual literature curation and genome-wide data mining. Nucleic Acids Research, 41(D1): D1055–D1062.
Zhao LY, Yao CC, Xing XY, et al. 2020. Single-cell analysis of developing and azoospermia human testicles reveals central role of Sertoli cells. Nature Communications, 11(1): 5683.
Zheng GXY, Terry JM, Belgrader P, et al. 2017. Massively parallel digital transcriptional profiling of single cells. Nature Communications, 8: 14049.
Zickler D, Kleckner N. 2016. A few of our favorite things: pairing, the bouquet, crossover interference and evolution of meiosis. Seminars in Cell & Developmental Biology, 54: 135–148.